EFFECTS OF PLASMA CONDITIONS ON DENSITY OF MICROCRYSTALLINE SILICON

A.C.W. Biebericher, A.R. Burgers, C. Devilee and W.J. Soppe
ECN Solar Energy, Thin Film PV-Technology
P.O. Box 1 NL-1755 ZG Petten

ABSTRACT: Micro-Wave PECVD with a linear plasma source is applied for deposition of intrinsic layers for µc-Si solar cells. An important advantage of the linear MW-PECVD method is the capability of large-area deposition of Si layers at high deposition rates. This makes MW-PECVD method a promising method for large-scale industrial fabrication of µc-Si and a-Si/µc-Si solar cells. A possible drawback of high deposition rate of µc-Si at low temperatures is the formation of layers with high porosity and high defect density. In this paper, the plasma geometry has been optimized to deposit more dense and less defective layers. The samples have been characterized by FTIR spectroscopy, Fourier Transform Photocurrent Spectroscopy (FTPS) and Raman spectroscopy. A program has been developed to fit the interference fringes in the FTIR spectra in order to eliminate the substrate background and to determine the refractive index of the Si layers. The plasma has been characterized by Optical Emission Spectroscopy. It appeared that the distance between the MW antenna and the substrate affects the post oxidation and the defect density of the material. Increasing this distance by about a factor 2 reduces the post oxidation rate by a factor of 6 and the defect density by a factor of 10 while the deposition rate decreases by about 40 %.

Keywords: Micro-crystalline silicon, PECVD, defect density.

1 INTRODUCTION

Microcrystalline silicon (µc-Si) is a very attractive material for fabrication of thin film silicon solar cells. So far, low deposition rates and lack of large area homogeneity provide 'barriers' for large-scale industrial fabrication of µc-Si based solar cells. At ECN, a linear plasma source is used to study Micro-Wave Plasma Enhanced Chemical Vapor Deposition (MW-PECVD) for deposition of intrinsic silicon layers for µc-Si solar cells. The MW plasma source provides large area deposition of µc-Si at high deposition rates. As such, the MW-PECVD method has shown to be a very promising method for large-scale industrial fabrication of µc-Si and a-Si/µc-Si solar cells. A common risk of µc-Si produced at high deposition rates in combination with low temperatures, is the presence of microvoids, resulting in a porous structure [1]. The porosity affects the electrical properties of the material, and therefore its behaviour in solar cells in a detrimental way. In this paper we present results of investigations for improving density and electronic quality of µc-Si layers.

2 EXPERIMENTAL SETUP

The depositions of intrinsic µc-Si i-layers were performed in a single-chamber reactor using a linear-microwave plasma source [2]. The deposition area amounts to 6 substrates of 10 cm × 10 cm. Typical settings are a pressure of 0.1 mbar, and a substrate temperature of 250 °C. The power was 2 × 500 W and the gas flows 200 sccm H_2, 15 sccm SiH_4, 0-50 sccm Ar. Gas purifiers are applied to ensure an impurity level of the gases better than 1 ppm. The deposition rate is of µc-Si is typically 0.6 - 1 nm/s.

Optical emission of the plasma was monitored by an Avantes spectrometer in the wavelength range from 200 - 1000 nm, with a resolution of 0.6 nm. Emitted light was collected through a saphire viewport in the reactor and was guided to the spectrometer through an optic fiber cable with high UV transmission. The viewport is positioned slightly above the level of the substrates in the default configuration (see below).

Raman scattering spectra are obtained in back-scattering mode, with incident laser light at a wavelength of 532 nm and with a resolution of 1 cm^{-1}.

FTIR spectra in the range 400 - 4000 cm^{-1} are recorded by a Perkin-Elmer BX-II spectrometer, at a resolution of 8 cm^{-1}. A computerprogram has been developed to fit the interference fringes in the FTIR spectra. This enables elimination of the background of the substrate, and allows determination of the refractive index of the layers in the infrared wavelength regime.

Microcrystalline silicon in general is less compact and more porous than c-Si and this porosity leads to lower refractive indices. FTIR measurements thus quickly provide information on the optical density and the porosity of the material.

We examined the effect of the distance between MW source and substrate for five different geometries, depicted in Figure 1. By varying the distance between source and substrate, we vary the 'remoteness' of the configuration. Basically, the (hydrogen) plasma is confined to a cylindrical zone around the MW antenna, where the pressure determines the extension of the plasma zone. By changing the distance between MW antenna and substrate, we change the plasma density at the level of the substrate (and SiH_4 gas shower). This has a strong effect on the total plasma chemistry.

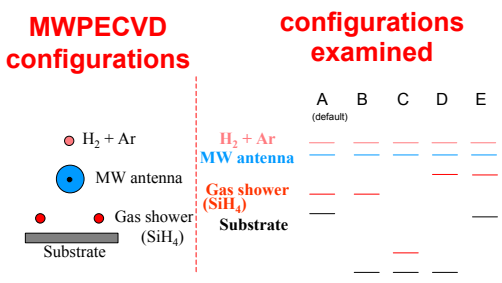

Figure 1: Micro-wave plasma source configurations.

3 OPTICAL ANALYSIS PROGRAM FOR FTIR

The FTIR samples consist of a mono-crystalline silicon wafer as substrate plus a microcrystalline silicon layer. The microcrystalline layer is about 1 µm thick and is thin compared to the wavelengths used in FTIR. Therefore, the IR transmission spectrum will show interference fringes if the refractive index of the layers *n(*l*)* is different from that of the substrate. The amplitude of the interference is a measure for the mismatch of the refractive indices, where the periodicity is determined by the product of refractive index and thickness of the layer.

We have developed a computer program to eliminate these interference fringes in order to enable an accurate determination of various bond densities in the layers. Simultaneously, this analyses provides us with the refractive index in the IR regime.

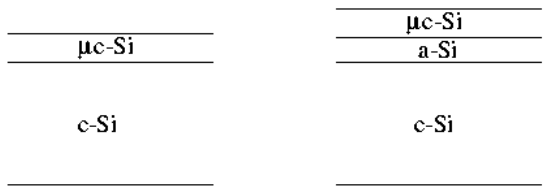

Figure 2: Multilayer configurations used in FTIR analysis program.

The transmission of a multi-layer system can be computed from the thickness of each layer and the *n(*l*)* and *k(*l*)* of each layer. The mathematical techniques to do this are described in textbooks [3,4]. The optical properties of mono-crystalline silicon are well known and were checked by a separate FTIR measurement. The microcrystalline layer is modelled with a constant refractive index or a refractive index that depends linearly on the wave number. The extinction coefficient of the microcrystalline layer in the IR wavelength range is assumed to be zero. The fitting is done in the regions in the FTIR wavelength range where there is no absorption in the microcrystalline layer: from 1340 cm^{-1} to 2000 cm^{-1} and from 2400 cm^{-1} to 4000 cm^{-1}.

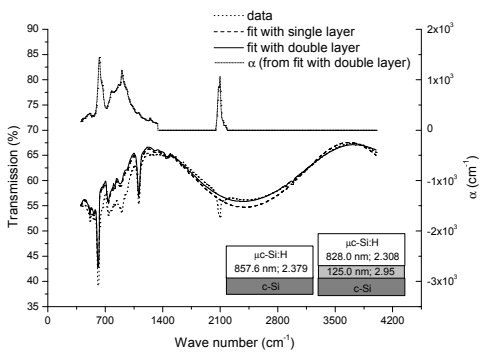

Figure 3: Fit of typical FTIR spectrum of µc-Si layer with single and double layer model.

For some cases (see Figure 3) we were unable to fit the data with a single layer model. In these cases we applied a double-layer model consisting of an amorphous incubation layer with thickness of typically 100 nm and refractive index of 2.95 plus a microcrystalline bulk layer.

It can be concluded that the refractive index of the deposited layer in some cases is not constant over the whole thickness of the layer and that the refractive index is higher for the incubation layer than for the bulk of the film.

Interference fringes were observed for all layers grown in these experiments. The mismatch between the refractive index of the layers (typically below 3.0) and that of the crystalline silicon wafer (3.4 in the IR regime) points at a certain porosity of the layers, which is probably caused by micro cracks along the crystalline columns.

4 RESULTS AND DISCUSSION

4.1 Crystal fraction determined by Raman spectroscopy

In the graph below, the crystal fraction (defined as I(520nm)/I(480 nm) is plotted versus the SiH_4 flow for layers grown with different plasma source geometries.

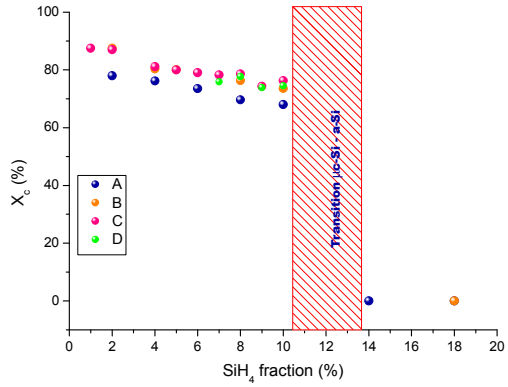

Figure 4: Crystal fractions of layers deposited in various MW source geometries.

Transition from µc-Si to a-Si seems to be independent of the plasma source geometry, and takes place at a SiH_4 fraction of about 11 %.

The deposition rate of µc-Si, close to the transition to a-Si is about 1 nm/s for the default geometry A, on an area of about 70×20 cm^2. Increasing the antenna-substrate distance leads to a decrease of the deposition rate by 40 % for geometry B, but this decrease is to some extent compensated by the increase of the effective deposition area.

4.2 Postoxidation

To obtain more insight in the effect of the plasma configuration on the rate of post oxidation (which is a measure for the density of the material) we monitored the IR aborption by Si-O bonds at 1060 cm^{-1} for a number of samples. The samples have been exposed to air and were measured almost every day, during the first week after deposition.

In Figure 5 we plotted results for samples deposited with different plasma geometries, where other deposition parameters (pressure, temperature, gas flows) were identical.

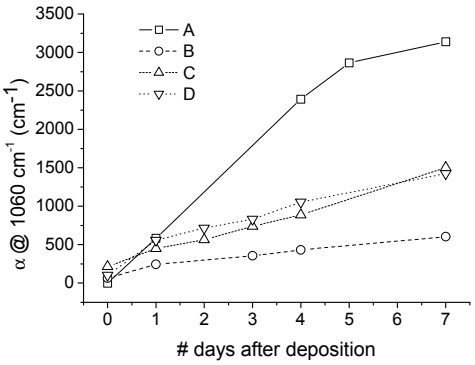

Figure 5: IR absorption of Si-O bonds at 1060 cm^{-1} as a function of time.

Configuration A is the default geometry (see Figure 1). It can be observed that the alternative geometries, with larger antenna-substrate distances, lead to a significant decrease of the post-oxidation rate. Best results (lowest oxidation rates) are obtained for configuration B. For this configuration the oxygen content of the layers after a week exposure to air, is more than a factor 6 smaller than for the default configuration A. Changing the position of the SiH_4 gas inlet (configurations C and D), leads to somewhat higher oxidation rates than for configuration B. In the next section, we will discuss possible plasma reactions that might be responsible for these phenomena.

4.3 Optical Emission Spectroscopy

In the graphs below, the light intensity of Si* at 251 and at 288 nm, SiH* at 412 nm, and H_α at 656 nm have been plotted as a function of the SiH_4 flow for the different plasma geometries

Emission by Si* (Figure 6 and Figure 7) and SiH* (Figure 8) is non-zero at zero flow of SiH_4. This must be a result of etching of silicon from the walls by hydrogen radicals. For configurations B, C and D (with larger antenna-substrate distances) this etching effect seems to dominate the concentration of Si* and SiH* species. The concentration of hydrogen radicals (e.g. H_α in Figure 9) also is larger for larger antenna-substrate distances. We conclude that the substrate table plus substrates is a high-recombination surface for hydrogen radicals.

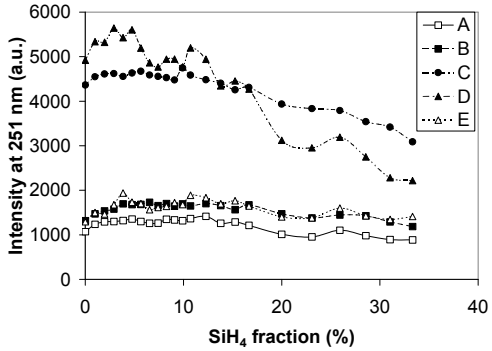

Figure 6: Light intensity emitted by Si* at 251 nm for different configurations.

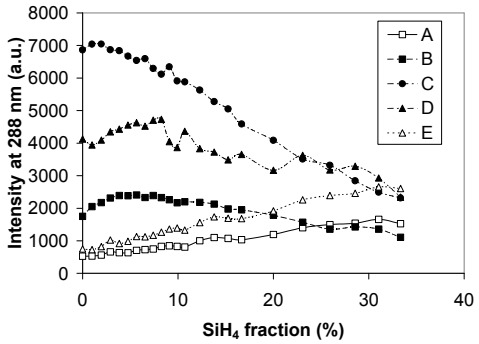

Figure 7: Light intensity emitted by Si* at 288 nm for different configurations.

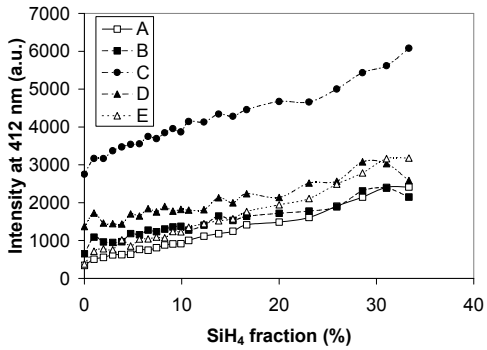

Figure 8: Light intensity emitted by SiH at 412 nm for different configurations.

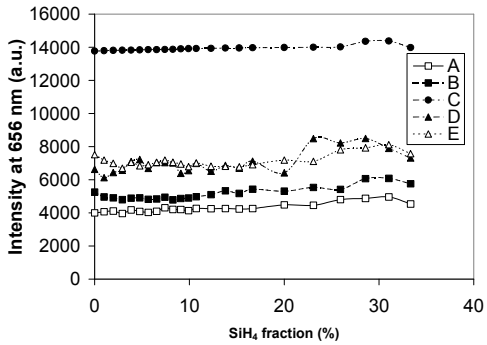

Figure 9: Light intensity emitted by H_α at 656 nm for different configurations.

The hydrogen radical concentration (Figure 9) increases only slightly with increasing SiH_4 flow. Basically, there are three dissociation channels for SiH_4 [5]:

$$SiH_4 + e \rightarrow SiH_2 + H_2 + e \quad (1)$$
$$SiH_4 + e \rightarrow SiH_3 + H + e \quad (2)$$
$$SiH_4 + H \rightarrow SiH_3 + H_2 \quad (3)$$

The weak increase of emission by H radicals with increasing SiH_4 flow indicates that reactions (2) and (3) are well in balance, such that the net production of H

radicals stems only from dissociation of hydrogen by electron impact:

$$H_2 + e \rightarrow 2H + e \qquad (4)$$

and therefore is almost constant since the H_2 flow was kept constant in these experiments.

It is generally assumed that the formation of compact silicon layers with low defect densities, by PECVD requires that the growth precursors predominantly consist of SiH_3 radicals and that Si, SiH and SiH_2 concentrations are as low as possible [6,7]. Following this argumentation, it is understandable why geometries C and D give rise to layers with larger post-oxidation rates than geometry B. Si* and SiH* concentrations are appreciably larger, and it is reasonable to assume that SiH_2 concentrations are larger too for geometries C and D.

In an attempt to understand why geometry B gives rise to denser layers than geometry A, it should be noted that the existence of a vertical gradient in the concentrations of Si* and SiH* is well possible. In other words it is plausible that the concentrations of Si* and SiH* are higher near the MW antenna than near the substrate, since a large fraction of these species stems from etching of parasitic silicon deposited on the walls and the quartz tube shielding the antenna.

Before Si and SiH (and SiH_2) species arrive at the substrate they can bind hydrogen by the following reactions [5]:

$$Si + H_2 \rightarrow SiH_2 \qquad (5)$$
$$SiH + H_2 \rightarrow SiH_3 \qquad (6)$$
$$SiH_2 + H \rightarrow SiH_3 \qquad (7)$$
$$Si + SiH_4 \rightarrow 2SiH_2 \qquad (8)$$

The probability of these reactions is related to the dwell time of the species. For larger antenna-substrate distances, the Si and SiH species require more time to travel from the zone that is monitored by optical emission to the substrate, so the probability that reactions (5) to (8) can occur is larger.

We conclude that geometry B allows the growth of denser layers than geometry A, because the larger distance between antenna and substrate induces a reduction of unwanted growth precursors Si, SiH and SiH_2 by hydrogen bonding through reactions (5)-(8).

Moving the SiH_4 gas shower from its default position (geometry B) to a position further from the MW antenna (geometry C) does not improve the layer density as established by the post-oxidation rate (Figure 5). One might have expected that geometry C would lead to an enhanced contribution of reaction (3) at the expense of reactions (1) and (2), leading to an enhanced fraction of desired SiH_3 species. Apparently the lifetime of H radicals is too short to enhance reaction (3) if the distance between antenna (where the H radicals are formed) and the SiH_4 gas inlet is increased.

4.4 Fourier Transform Photo Spectroscopy

A number of samples have been characterized by Fourier Transform Photo-current Spectroscopy (FTPS)[8]. In Figure 10 the spectra are shown for samples grown with plasma source geometries A and B. It is clear that the increase of the antenna-subtrate distance helps to improve the quality of the layers: the value of α @ 0.8 eV is 10 times lower for layer grown with geometry B.

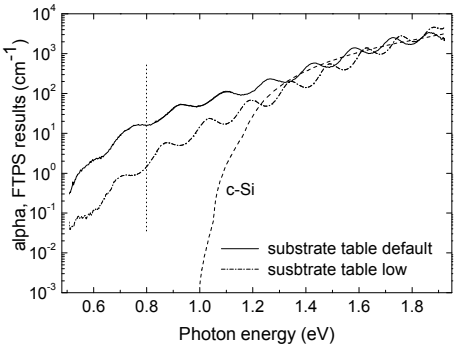

Figure 10: FTPS curves for samples deposited with geometries A and B.

5 CONCLUSIONS

The MW plasma source geometry strongly affects the material density but does not affect the crystal fraction. Increase of the source-substrate distance leads to reduction of post-oxidation by a factor 6 and to reduction of the defect density by a factor 10, while the deposition rate decreases by about 40 %. The improvement of material quality is probably a result of enhanced hydrogen binding by reactive SiH_x ($x<3$) radicals generated in the vicinity of the MW antenna. Increase of the distance between MW antenna and SiH_4 gas shower does not lead to improved quality of the layers. The lifetime of H radicals in such a configuration probably is too short to enable a larger production of desired SiH_3 growth precursors through the reaction $SiH_4 + H \rightarrow SiH_3 + H_2$.

6 REFERENCES

[1] C. Smit et al, Proc. 29th IEEE PVSC, New Orleans, (2002) 1170.
[2] W.J. Soppe, A.C.W. Biebericher, C. Devilee, H. Donker, H. Schlemm, Proceedings of 3rd World Conference of Photovoltaic Energy Convention (2003) 5P-A9-13.
[3] E. Hecht and A. Zajac, Optics, Addison-Wesley, 6th edition (1980).
[4] H.A. MacLeod, Thin Film Optical Filters, Adam Hilger (1986).
[5] M.J. Kushner, J. Appl. Phys. **63** 2532 (1988).
[6] J.R. Abelson, Appl. Phys. A: Solids Surf. **56**, 493 (1993).
[7] S Sriraman and E.S. Aydil, J. Appl. Phys. **95,** 1792 (2004).
[8] M. Vaneček and A. Poruba, Appl. Phys. Lett. **80** (5), 719 (2002).